THE JOURNAL OF PHYSICAL CHEMISTRY A

Article

pubs.acs.org/JPCA

Photoinduced Electron Transfer through Peptide-Based Self-Assembled Monolayers Chemisorbed on Gold Electrodes: Directing the Flow-in and Flow-out of Electrons through Peptide Helices

Mariano Venanzi,*[,†] Emanuela Gatto,[†] Mario Caruso,[†] Alessandro Porchetta,[†] Fernando Formaggio,[‡] and Claudio Toniolo[‡]

[†]Department of Chemical Sciences and Technologies, University of Rome "Tor Vergata", 00133 Rome, Italy

[‡]Institute of Biomolecular Chemistry, Padova Unit, CNR, Department of Chemistry, University of Padova, 35131 Padova, Italy

Supporting Information

ABSTRACT: Photoinduced electron transfer (PET) experiments have been carried out on peptide self-assembled monolayers (SAM) chemisorbed on a gold substrate. The oligopeptide building block was exclusively formed by C^{α}-tetrasubstituted α-aminoisobutyric residues to attain a helical conformation despite the shortness of the peptide chain. Furthermore, it was functionalized at the C-terminus by a pyrene choromophore to enhance the UV photon capture cross-section of the compound and by a lipoic group at the N-terminus for linking to gold substrates. Electron transfer across the peptide SAM has been studied by photocurrent generation experiments in an electrochemical cell employing a gold substrate modified by chemisorption of a peptide SAM as a working electrode and by steady-state and time-resolved fluorescence experiments in solution and on a gold-coated glass. The results show that the electronic flow through the peptide bridge is strongly asymmetric; i.e., PET from the C-terminus to gold is highly favored with respect to PET in the opposite direction. This effect arises from the polarity of the Au−S linkage ($Au^{\delta+}$−$S^{\delta-}$, *junction effect*) and from the electrostatic field generated by the peptide helix.

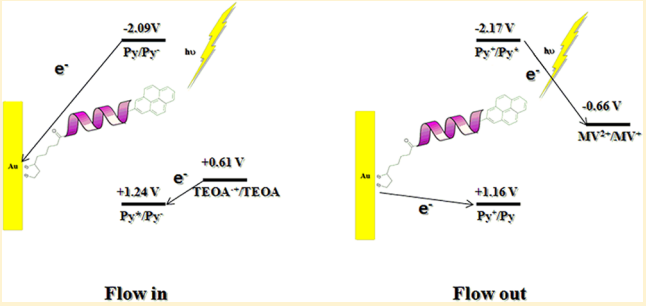

INTRODUCTION

Electron transfer (ET) studies on peptide scaffolds functionalized with ET donor (D)−acceptor (A) pairs have shown that peptides are able to promote long-range ET with great efficiency,[1−4] especially when the peptide backbone attains a helical conformation.[5,6] In particular, the amide n and π orbitals are thought to represent the stepping stones on the pathway that electrons pursuit flowing from the D to the A states across the peptide chain.[7−10] However, although ET studies on D−peptide−A systems have almost clarified the molecular details of ET in solution, an understanding of such processes in hybrid systems composed of electroactive peptides immobilized on conductive or semiconductive surfaces is still inadequate.[11,12]

Peptide-based self-assembled monolayers (SAMs) chemisorbed on a gold substrate through Au−S linkages represent a suitable model for improving our knowledge of ET at the interface between an organic layer and an electrode surface. For this reason, peptide SAMs have been extensively investigated by microscopy techniques with atomic resolution, and spectroscopic, electrochemical and photoelectrochemical methods.[13−31] This intense research effort has been shedding light on the role of structural (i.e., the secondary structure attained by the peptide matrix) and electronic effects (i.e., the coupling between the D and A states through the electronic states of the peptide bridge) in determining the ET efficiency.

In this contribution, the results of photocurrent generation (PG) experiments, i.e., the production of a net electronic current upon electromagnetic excitation, carried out on a SAM formed by conformationally constrained peptide building blocks are presented. The rationale for using this unique class of peptides is that the rate of photoinduced electron transfer (PET) exponentially decreases with increasing the distance of the photoactive group from the electrode. On the other hand, photoexcited chromophores too close to the gold surface are generally rapidly quenched by energy transfer and/or fast charge-recombination to the metal of the photoinduced charge-separated pair. An optimal distance should be therefore attained, balancing accurately the efficiency of competitive electron and energy-transfer processes and maximizing the lifetime of the charge-separated state. Unfortunately, when short alkanethiols or oligopeptides formed by the coded amino acids are used, disordered organic films are generally obtained, because of the large number of different conformations populated by the polymer chains. In this case, most of the

Special Issue: Franco Gianturco Festschrift

Received: April 17, 2014
Revised: June 5, 2014
Published: June 5, 2014

dx.doi.org/10.1021/jp503791w | J. Phys. Chem. A 2014, 118, 6674−6684

excitation energy is lost by energy transfer to the surface, due to the high mobility of the polymer chains that enables the chromophores to reach contact distances with the metal surface.

It is well-known that the electronic conductivity of peptides is strongly enhanced when the peptide chain is folded in a helical structure.[5,6] In this case, the dipole moments associated with each peptide bond sum up to give rise to a large macrodipole, the electrostatic field of which heavily affects the direction and the efficiency of the ET process.[32−34] The demanding and, in principle, conflicting requirement to build up helically ordered oligopeptides has been accomplished by peptide chemistry through the synthesis of noncoded amino acids, showing highly reduced conformational mobility (*peptide foldamers*).[35,36] This is the case for C^{α}-tetrasubstituted residues, i.e., α-amino acids with an alkyl group substituting the hydrogen atom on the C^{α}. The α-aminoisobutyric acid (denoted as Aib or U in a three- or single letter code, respectively), characterized by a *gem*-dimethyl substitution on the C^{α} atom, is the prototype of these exotic amino acids.[37,38]

The peptides investigated in this contribution are exclusively formed by Aib residues. Aib-rich peptides have been shown to populate predominantly 3_{10}- or α-helical structures depending on the length of the peptide chain, the transition between the two secondary structures being usually found for a number of residues comprised between n = 7 and 8.[36−40] The peptides investigated here were functionalized at the N-terminus with the lipoyl moiety for stable bidentate binding on gold, by exploiting the strong Au−S affinity (≈40 kcal·mol^{-1}) between the gold surface and the lipoyl disulfide group. Interestingly, SAMs formed by peptides functionalized with a thiol group at the N-terminus and chemisorbed on gold surfaces have shown improved stability with respect to thiol C-terminated peptides, as a result of the electrostatic field associated with the peptide helix and the polar character of the Au(δ^+)−S(δ^-) linkage.[41,42] A further issue to be faced in this type of studies is to enhance the efficiency of the photon capture cross-section of the peptide SAM. The optical transitions of the peptide group occur in the far UV region, peaking at 220 nm for the weak n → π^* transition and 190 nm for the allowed $\pi \rightarrow \pi^*$ transition. Unfortunately, at these wavelengths, direct photoemission from gold largely predominates, which inhibits the chance to investigate the conductive properties of the peptide spacer by PG experiments. For this reason, the peptide under scrutiny in this work was further functionalized at the C-terminus with a 1-pyrene (Py) chromophore, characterized by strong absorption and high-fluorescence quantum yield in the near UV−vis regions.

In the following, we will use the acronyms SSU6Py for the pyrene functionalized hexapeptide and SSU6 for the same $(Aib)_n$ homohexapeptide lacking the pyrene chromophore (Scheme 1). The latter was employed as a reference compound in the PG experiments. The capacity of SSU6Py to form a densely packed SAM on a gold surface was already demonstrated, as well as its electrochemical and photocurrent properties under anodic conditions, i.e., ET from the pyrene excited state to gold in the presence of an electron donor in solution.[24,25] Very recently, a TiO_2/Au/SSU6Py photoactive unit was implemented in a prototype dye-sensitized solar cell, showing enhanced incident photons-to-current efficiency (IPCE).[43] Here, we report on a detailed comparison between the results of PG experiments carried out in the presence of an electron acceptor (anodic current conditions) or an electron donor (cathodic current conditions) in solution. These experiments have been performed in a Grätzel-like electrochemical cell, using a gold electrode modified by chemisorptions of an SSU6Py or an SSU6 SAM as a working electrode. Steady-state and time-resolved fluorescence experiments have been also carried out in solution and on supported peptide films to prove the excited-state origin of the ET process and measure the ET rate constants associated with the Py*/electron donor and Py*/electron acceptor interactions.

Scheme 1. Chemical Structures and Acronyms of the Two Peptides Investigated

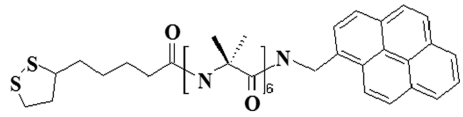

SSU6Py

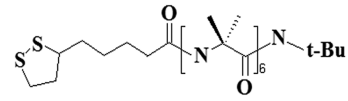

SSU6

MATERIALS AND METHODS

Materials. Synthesis and characterization of the peptides SSU6Pyr and SSU6 were already reported elsewhere.[24,25] Spectrograde solvents (Carlo Erba, Milan, Italy) were exclusively used for all experiments. Water was distilled and passed through a Milli-Q purification system. Other chemicals, triethanolamine (TEOA) (Fluka, Buchs, Switzerland), potassium chloride, sodium sulfate (Carlo Erba, Milan, Italy), potassium ferricyanide and methylviologen (MV^{2+}) dichloride (Aldrich, Buchs, Switzerland) were all of reagent grade quality and used without further purification.

Preparation of Self-Assembled Peptide Thin Films. Gold electrodes were etched for 15 min in a freshly prepared piranha solution (2:1 sulfuric acid/H_2O_2, v/v), rinsed with bidistilled water and ethanol (5 times each) before immersion in the peptide solution for the SAM deposition. SAM-coated electrodes were prepared by dipping a gold electrode into a 1 mM ethanol solution of the peptide in a N_2 atmosphere. After 18 h, the electrode was repeatedly rinsed with ethanol to remove physically adsorbed peptides from the SAM and dried for 3 min under a gentle argon flow. The surface coverage of the peptide film was estimated by cyclic voltammetry (CV) measurements in 0.5 M NaOH, integrating the irreversible reduction peak of the Au−S linkage (−0.9 V).[44] The effective surface area of the Au electrode was determined by CV measurements quantifying the discharge of a $K_3[Fe(CN)_6]$ standard solution by following the Randles−Sevcik equation:[45]

$$i_p = 0.4463nFAC(nF\nu D/RT)^{1/2}$$

where i_p is the current maximum, n is the number of electrons transferred in the redox event, A is the electrode area in cm^2, F is the Faraday constant, D is the ferricyanide diffusion coefficient (7.2×10^6 cm^2/s), C is the electrolyte concentration, and ν is the scan rate. By plotting i_p as a function of $\nu^{1/2}$, we determined the electrode active surface (0.90 ± 0.05 cm^2) and found it to be 3.6 times larger than the geometric surface area (0.25 cm^2) of the electrode.

dx.doi.org/10.1021/jp503791w | J. Phys. Chem. A 2014, 118, 6674−6684

Electrochemistry. Cyclic voltammograms were obtained by using a PG-310 potentiostat (Heka Elektronik, Lambrecht/Pfalz, Germany). CV experiments were carried out at room temperature, adopting a standard three-electrode configuration with a SAM-coated gold plate as the working electrode, a platinum wire as the auxiliary electrode, and Ag/AgCl as the reference electrode. Blocking experiments were carried out with a 0.5 mM $K_3Fe(CN)_6$ solution in 1 M KCl at a sweep rate of 50 $mV{\cdot}s^{-1}$. Photocurrent measurements were performed at room temperature using the three-electrode setup described above, by using Na_2SO_4 (0.1 M) as the supporting electrolyte and TEOA (at 50 mM concentration) as the electron donor in solution. Otherwise, 50 mM MV^{2+} ethanol solutions were used for PG experiments under cathodic conditions. In these experiments, the SAM-modified working electrode was irradiated with a Xe lamp (150 W) equipped with a monochromator and the generated photocurrent was detected by the voltammetric analyzer described above. The IPCE value was determined by using the following equation:[46]

$$\text{IPCE}\ (\%) = \frac{100i\ (\text{A/cm}^2)\ 1240}{I\ (\text{W/cm}^2)\ \lambda\ (\text{nm})}$$

where i is the measured photocurrent, I is the incident light power density, and λ is the incident wavelength (340 nm). The intensity of the incident light was evaluated by azobenzene actinometry.[47]

Fluorescence Spectroscopy. Emission spectra at micromolar concentrations were obtained on a Spex-Fluoromax2 (Horiba Jobin-Yvon Instruments, Longjumeau, France) spectrofluorimeter, equipped with a 150 W xenon lamp operating in single photon counting (SPC) mode. Samples were excited at 340 nm and the fluorescence spectra recorded from 360 to 500 nm using a bandwidth of 5 nm for both excitation and emission slits. Fluorescence time decays were obtained by use of an EAI Life-Spec-ps (Edinburgh Analytical Instruments, Edinburgh, U.K.), operating in the SPC mode (λ_{exc} = 340 nm; λ_{em} = 397 nm; time interval = 500 ns; channels = 2048; excitation/emission bandwidths = 8 nm). Excitation at λ = 340 nm was obtained by an IBH NanoLED light emitting diode (Horiba Jobin-Yvon Instruments) with 1 ns pulse duration. Experimental time decays were deconvoluted by the pulsed excitation profile by standard software provided by EAI and based on discrete multiexponential analysis.

RESULTS AND DISCUSSION

Cyclic Voltammetry (CV). Formation of SSU6Py and SSU6 SAMs on a gold electrode was checked by CV measurements in the presence of an electrochemical standard redox species [$K_3Fe(CN)_6$, $E°$(0.36 V)]. The chemisorption of the peptide film passivates the gold surface, inhibiting the discharge of the redox pair to the electrode (blocking experiment). The decreased activity of the redox pair can be considered as an estimate of the coverage extent and the packing density of the peptide film on the gold surface. This effect is clearly shown in Figure 1, where the voltammograms measured for the bare gold electrode and the electrode modified by the SSU6Py and the SSU6 SAMs are reported. The residual current intensity measured using the modified electrodes can be ascribed to the capacitive current caused by the electrolyte (KCl) diffusion to the electrode. This result also means that the peptide SAM did not completely passivate the electrode surface, allowing for the formation of a double-layer

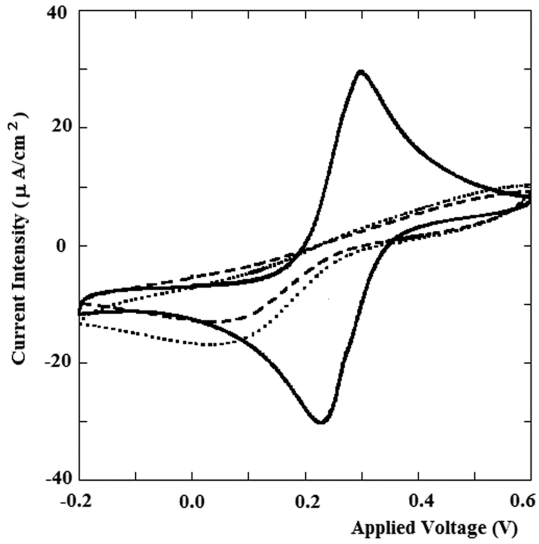

Figure 1. CV experiments in a 50 mM $K_3Fe(CN)_6$ solution (blocking experiment). The three curves are obtained by using a bare gold electrode (full line) as a working electrode, or a gold electrode modified by chemisorption of the SSU6Py (dotted line) or SSU6 (dashed line) SAM.

at the organic/metal interface as a consequence of the applied voltage.

It should be stressed that the structure of the double-layer at the electrode surface is strongly affected by the peptide SAM, for two reasons: (i) the polar nature of the Au−S interaction, which confers to the Au−S bond a marked electrostatic character,[48] and (ii) the electrostatic field associated with the peptide helix macrodipole.[28,49,50] As already claimed in the Introduction, the helix itself, due the polar character of the peptide bond (3.6 D), gives rise to an electrostatic field that deeply affects the local electrochemical properties of the peptide layer and, as a result, the efficiency of ET across the peptide chain. CV experiments also showed that SSU6Py is subjected to an irreversible oxidation reaction at +1.0 V applied potential (Supporting Information, Figure SI1). Subsequently, a new peak at 0.2−0.4 V can be observed, most likely ascribable to the discharge of diol/diketone species, namely the stable byproducts of the pyrene oxidation. This peak could be still observed after repeated scans, indicating the integrity of the peptide film on the gold surface at these applied potentials.

By measuring the total charge exchange accompanying the oxidation of the pyrene chromophore, we estimated a density of the SSU6Py SAM on the electrode surface equal to 1.3×10^{-10} mol/cm^2. This value is in good agreement with that obtained by assuming a close hexagonal packing of the helical peptides on the surface, with a tilt angle of 40−50° with respect to the normal to the gold surface. This finding confirms the high-density surface coverage of the gold electrode by the SSU6Py SAM and suggests that the peptide building blocks attain an almost vertical orientation with respect to the gold surface.

Photocurrent Generation (PG) Experiments. PG experiments were carried out in a three-electrode electrochemical cell in the presence of an electron donor (TEOA) or an electron acceptor (MV^{2+}) species in solution under the same experimental conditions. The energetics of the cell under anodic and cathodic conditions is depicted in Scheme 2. Upon photoexcitation of the (Au)SSU6Py SAM in a 50 mM TEOA solution with UV−vis irradiation from 300 to 450 nm at a null

dx.doi.org/10.1021/jp503791w | J. Phys. Chem. A 2014, 118, 6674−6684

Scheme 2. Energetics and Photo-electrochemical Processes under Anodic (Left) and Cathodic (Right) Conditions

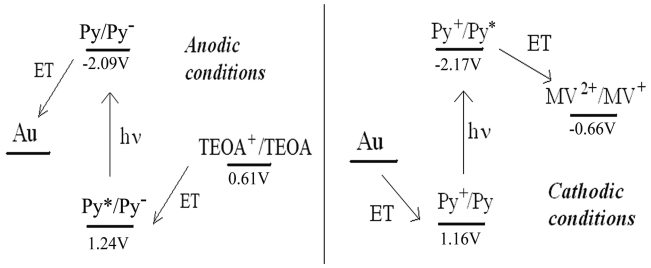

applied overpotential, a nanoAmpère (nA) anodic current was obtained. Examples of the photocurrents obtained at the different excitation wavelengths are reported in Figure 2A. The

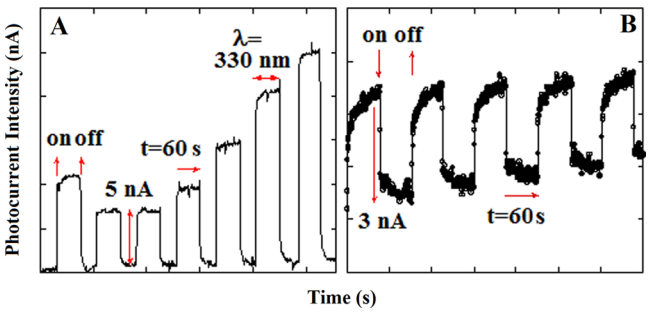

Figure 2. Photocurrent measured for a gold electrode modified by deposition of the SSU6Py SAM. A: Anodic conditions (TEOA, 50 mM). B: Cathodic conditions (MV^{2+}, 50 mM).

almost instantaneous rise (drop) of the measured photocurrent upon the switch on (off) of photoexcitation can be readily appreciated within the time resolution of the present experiment (millisecond).

The elementary steps of the anodic photocurrent process can be briefly summarized as follows: (i) Excitation of the pyrene chromophore: the photon absorption event can be considered instantaneous on the time scale of both the electrochemical current production and ET processes at the molecular level. (ii) ET from TEOA (electron donor) to the excited pyrene [$E°(Py*/Py^{-\bullet}) = 1.24$ V]:

$$(Au)SSU6Py* + TEOA \rightleftarrows (Au)SSU6Py^{-\bullet} + TEOA^{+\bullet}$$

followed by reduction of $TEOA^{+\bullet}$ to the cathode [$E°(TEOA^{+}/TEOA) = 0.61$ V]. This step can be viewed as relatively fast due to the high bimolecular rate constants of the process (see at the time-resolved fluorescence experiments reported in the following), the high concentration of TEOA (50 mM), and the easy access of the reactant to the Py* acceptor, suitably positioned at the outer layer of the peptide SAM. The intramolecular ET from the $Py^{-\bullet}$ radical anion [$E°(Py/Py^{-\bullet}) = -2.09$ V] to the Fermi level of the gold surface:

$$(Au)SSU6Py^{-\bullet} \rightleftarrows {}^{-}(Au)SSU6Py \quad (1)$$

is most likely the time-determining step, as it requires superexchange-assisted ET through the peptide chain. The outcome of the three elementary processes outlined above is a net electronic current to the gold electrode (anode).

The results of the same experiment carried out in a 50 mM MV^{2+} solution are reported in Figure 2B, where the onset of a negative (cathodic) current for different excitation wavelengths can be observed. In this case, upon instantaneous excitation of the pyrene chromophore, a fast ET from the pyrene excited state [$E°(Py^{+}/Py*) = -2.17$ V] to the MV^{2+} acceptor in solution [$E°(MV^{2+}/MV^{+}) = -0.66$ V], takes place:

$$(Au)SSU6Py* + MV^{2+} \rightleftarrows (Au)SSU6Py^{+\bullet} + MV^{+}$$

This step can be considered very fast on the same bases of the PG experiment carried out under anodic condition described above, i.e., high ET bimolecular rate constants, high MV^{2+} concentration, and easy access to Py*. The time-determining step involves an intramolecular ET from the gold surface to the $Py^{+\bullet}$ radical cation [$E°(Py^{+}/Py) = 1.16$ V] through the peptide chain, i.e.

$$(Au)SSU6Py^{+\bullet} + e^{-} \rightleftarrows (Au)SSU6Py \quad (2)$$

Oxidation of MV^{+} to the anode closes the circuit, resulting in a net cathodic current.

It should be noted that the two ET steps through the peptide chain under anodic and cathodic conditions are not equivalent.

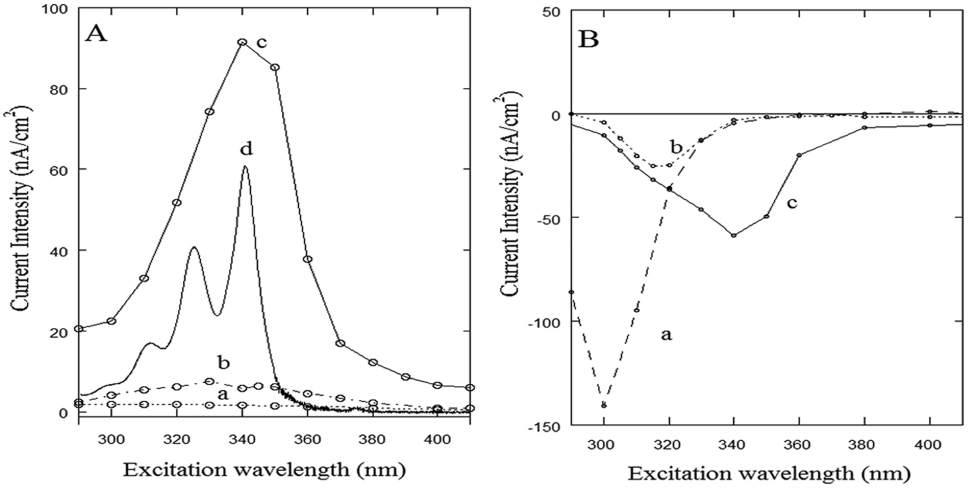

Figure 3. Photocurrent action spectra under anodic (A) and cathodic (B) conditions: (a) bare gold electrode; (b) Au/SSU6 electrode; (c) Au/SSU6Py electrode. In (A) the absorption spectrum of pyrene in ethanol is also reported for comparison (d).

dx.doi.org/10.1021/jp503791w | J. Phys. Chem. A 2014, 118, 6674−6684

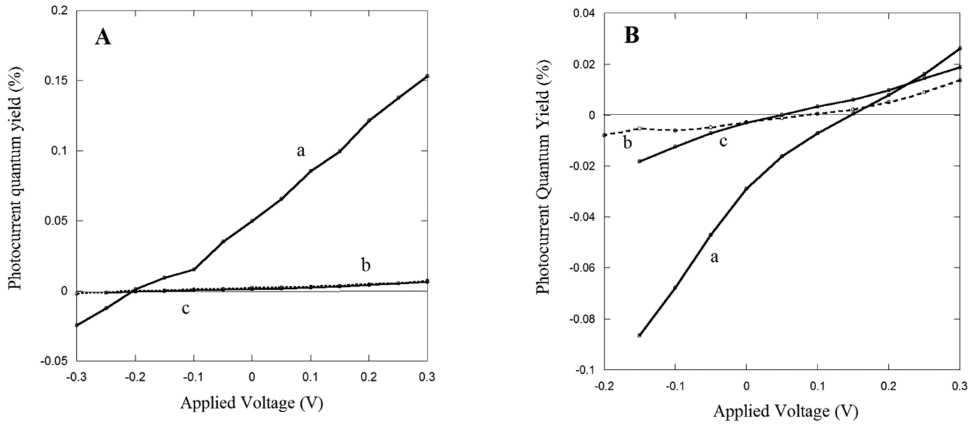

Figure 4. Photocurrent quantum yield (%) versus the applied voltage for anodic (A) and cathodic (B) conditions: (a) gold electrode modified by the SSU6Py SAM; (b) gold electrode modified by the SSU6 SAM; (c) bare gold electrode. The excitation wavelength is λ_{exc} = 340 nm in all cases.

In the former case (eq 1), electrons flow from the peptide negative C-terminus to the positive N-terminus, i.e., along the favorable electrostatic field generated by the peptide helix (3.6 D per residue). In the latter (eq 2), the electrons flow in the opposite direction, i.e., against the helical peptide macrodipole polarity. Besides that, the Au−S linkage features a marked charge-transfer character, i.e., $Au^{\delta+}-S^{\delta-}$, that significantly lowers the charge injection barrier to the gold surface at the organic−metal junction. Both effects make ET from Py* to the gold surface by far more efficient than ET in the opposite direction.

To verify this point, we carried out PG experiments with the same three-electrode apparatus in an equimolar TEOA/MV^{2+} solution. In this case, a predominant anodic current was obtained at all applied overpotentials (Supporting Information, Figure SI2).

According to the mechanisms outlined above, the photocurrent action spectra, i.e., the dependence of the photocurrent intensity on the excitation wavelength, under both anodic and cathodic conditions should overlap the absorption spectrum of the pyrene photosensitizer. This is exactly what is shown in Figure 3A, where the photocurrent action spectrum under anodic conditions and the absorption spectrum in ethanol of SSU6Py are reported. It should be noted that illuminating the bare gold electrode in the wavelength region between 280 and 410 nm did not produce any significant electronic current. On the contrary, high-intensity electronic currents were obtained under illumination below 260 nm as a result of a direct photoelectron emission from the gold surface, the work function of which is comprised between 5.1 and 5.5 eV, or of electrochemical processes originated by photoexcited TEOA. In Figure 3B the photocurrent action spectra of SSU6Py and SSU6 under cathodic conditions are reported together with the action spectrum of the bare gold electrode in a MV^{2+} solution for comparison. As can be seen, the long-wavelength component of the action spectrum of SSU6Py almost mirrors the action spectrum measured under anodic conditions. At shorter wavelengths, the action spectrum of the reference compound SSU6 reveals a cathodic photocurrent between 290 and 320 nm, ascribable to ET from Au to the photoexcited MV^{2+} [$E^{\circ}(MV^{2+}*/MV^{+} \approx 3$ V)]. At λ < 280 nm the absorption of the 50 mM MV^{2+} solution (λ_{max} = 260 nm) is so strong that excitation of molecules in the proximity of the electrode surface is totally inhibited by solution filter effect. Interestingly, the MV^{2+} photoactivity is partially inhibited by the presence of the peptide film, as can be observed by comparing the photocurrent spectra measured for the bare gold electrode and for the gold electrode modified by deposition of the SSU6 and SSU6Py monolayers (Figure 3B).

Therefore, the photocurrent action spectrum of the SSU6Py SAM under cathodic conditions results from the overlap of the current generated by photoexciting MV^{2+} at lower wavelengths (λ < 320 nm) and the current properly ascribable to photoinduced ET from the pyrene excited state at longer wavelengths (320 nm < λ < 400 nm).

It is mostly instructive to consider the dependence of the photocurrent intensity on the applied potential (P/V curve) at the gold electrode. The P/V curves obtained under anodic conditions at λ_{exc} = 340 nm for a bare gold electrode and a gold electrode modified by deposition of an SSU6Py or an SSU6 film, are reported in Figure 4A for comparison. The relevant photosensitizing effect caused by the pyrene-enhanced capture of excitation energy can be clearly spotted. The P/V plot shows that the anodic current generated by excitation of the SSU6Py SAM steadily increases as the positive applied potential increases, as a result of the larger energy difference between $Py^{-\bullet}$ and the Au Fermi level. Undoubtedly, we are in the normal Marcus region of the ET reaction. Interestingly, at negative applied potentials (V < −0.2 V), the inversion from anodic to cathodic currents can be observed.

This effect can be explained by taking into account that ET across the peptide SAM is most likely the time-determining step for both anodic (V > −0.2 V) and cathodic (V < −0.2 V) conditions. This is because the Py−Au distance, due to the rigid helical structure of the building blocks forming the peptide SAM, is around 20 Å, and the through-bond kinetic rate constant, exponentially decreasing with such a distance, is definitely slower than the bimolecular Py*/TEOA rate constant, mainly controlled by diffusion, as demonstrated by the time-resolved fluorescence experiments reported below.

Under these conditions the reaction at the electrode can be phenomenologically described by the Butler−Volmer equation:[45]

$$i = i_0\left(e^{[(1-\alpha)nF]/[RT(E-E^0)]} - e^{(-\alpha nF/RT)(E-E^0)}\right)$$

where i_0 is the exchange current, α is the ET transmission coefficient, and E is the applied potential. At very low overpotentials ($E \sim E^{\circ}$), one easily obtains

dx.doi.org/10.1021/jp503791w | J. Phys. Chem. A 2014, 118, 6674−6684

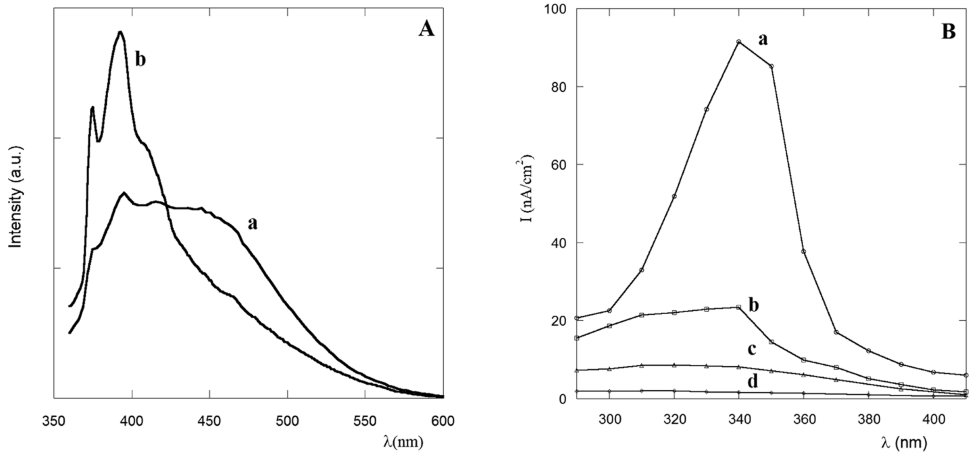

Figure 5. (A) Fluorescence spectra of SSU6Py (a) and SSU6/SSU6Py 10:1 (b) films on a gold coated glass. (B) Photocurrent action spectra under anodic conditions: (a) SSU6Py; (b) 10:1 SSU6/SSU6Py; (c) SSU6; (d) gold.

$$i \approx i_0 \frac{nF}{RT}(E - E^\circ)$$

i.e., the current is linearly proportional to the applied potential, and its sign reversed from anodic ($i > 0$) to cathodic ($i < 0$) currents at a characteristic zero-current potential E_{zcp} ($i_{zpc} = 0$).

Interestingly, in the case of the SSU6Py SAM $E_{zcp} = -0.25$ V, which means that the transition from anodic to cathodic currents is shifted to negative applied potentials; i.e., ET from pyrene to gold is favored over ET in the reverse direction. This effect may be ascribed to the combined effect of the helix macrodipole and the Au($\delta+$)−S($\delta-$) junction polarity that promote ET from the C- to the N-terminus. As shown by Kimura et al., for peptides linked to gold through the N-terminus, the two effects sum up conferring to the ET process strong directional properties.[49,51] The potential drop at the Au−S junction, measured by Au-linked alkanethiol, was estimated to be about −150 mV. In our case, the additional potential drop ascribable to the helix dipole electrostatic field should be therefore about −100 mV. This value should be compared with −140 mV obtained for a carbazole-dodecapeptide linked to a gold substrate through the same lipoic group.[13]

We assign the very weak electronic currents measured for the bare gold electrode and the gold electrode modified by deposition of the SSU6 SAM (2 orders of magnitude lower than the photocurrent generated by photoexcitation of the SSU6Py SAM) to a photothermal effect, recently described by Kraatz and co-workers.[52] In that case, a bare gold electrode and a gold electrode modified by a peptide SAM were illuminated by a very intense laser radiation and the electronic current generated was ascribed to the heating of the illuminated surface, which gives rise to a temperature gradient through the double-layer at the electrode/organic interface.

The dependence of the photocurrent intensity on the applied potential can be calculated on the basis of the difference between the rate constants associated with the opposite ET reactions, i.e., from $Py^{-\bullet}$ to gold (anodic current) and from gold to $Py^{+\bullet}$ (cathodic current):

$$i_{pc} = N_{Py^*}\left(\frac{k_{Py^{-\bullet}-Au} - k_{Au-Py^{+\bullet}}}{k_{Py^{-\bullet}-Au} + k_{Au-Py^{+\bullet}}}\right)$$

The rate constant for interfacial ET from a metal electrode to a bound redox group in the weak electronic coupling (nonadiabatic) regime can be written as (k_+ = anodic; k_- = cathodic):[53]

$$k_\pm = \sqrt{\frac{\pi}{\lambda k_b T}}\frac{\rho_{Au}(\varepsilon_F)}{\hbar} \times \int_{-\infty}^{+\infty} |H_{DA}(\varepsilon)|^2 \exp\left[-\frac{(\lambda \pm (E - E^\circ)e - \varepsilon)^2}{4\lambda k_b T}\right] f(\varepsilon)\, d\varepsilon$$

where $\rho_{Au}(\varepsilon_F)$ is the electronic states density at the Fermi level (assumed independent of energy; 0.3 per eV for Au), H_{DA} is the donor−acceptor electronic coupling matrix, λ is the reorganization energy, and ε is the electrode energy level, the population of which is determined by the Fermi−Dirac distribution function $f(\varepsilon)$. H_{DA} decreases exponentially with the D···A distance through the coupling parameter β, and H^0_{DA} is the electronic coupling matrix at contact distance.

$$|H_{DA}|^2 = |H^0_{DA}|^2 \exp(-\beta r)$$

β is a measure of the long-range efficiency of ET and strongly depends on the overlap between the donor and acceptor electronic states mediated by the peptide bridging units. In the case of ET through a peptide chain, the n and π orbitals of the amide bond were claimed to mediate the ET process as virtual electronic states (*superexchange* model) or temporary sites of residence for a transient electron (*hopping* model). Both models forecast a linear relationship between the ET rate constant and the squared electronic coupling matrix at low applied potentials.[54]

The P/V spectra of a bare gold electrode and a gold electrode modified by the SSU6 or SSU6Py SAM under cathodic conditions are reported in Figure 4B. Mirroring what observed in a TEOA solution, the cathodic (negative) current intensity increases as the negative applied voltage increases, as a result of the larger driving force for ET from Au to the pyrene ion radical ground state. At less negative overpotentials, the photocurrent intensity decreases, until the inversion from cathodic to anodic current is obtained for slightly positive overpotentials for both the SSU6 and SSU6Py SAMs [E_{zcp} = +0.1 and +0.15 V, respectively]. This effect again may be ascribed to the combined effect of the peptide helix dipole and to the Au−S link polarity, this time discouraging ET from gold to pyrene across the peptide chain. The +150 mV found for SSU6Py well compares with the +50 mV found by Kimura et al. for a lipoic-dodecapeptide linked to gold at the C-terminus,

dx.doi.org/10.1021/jp503791w | J. Phys. Chem. A 2014, 118, 6674−6684

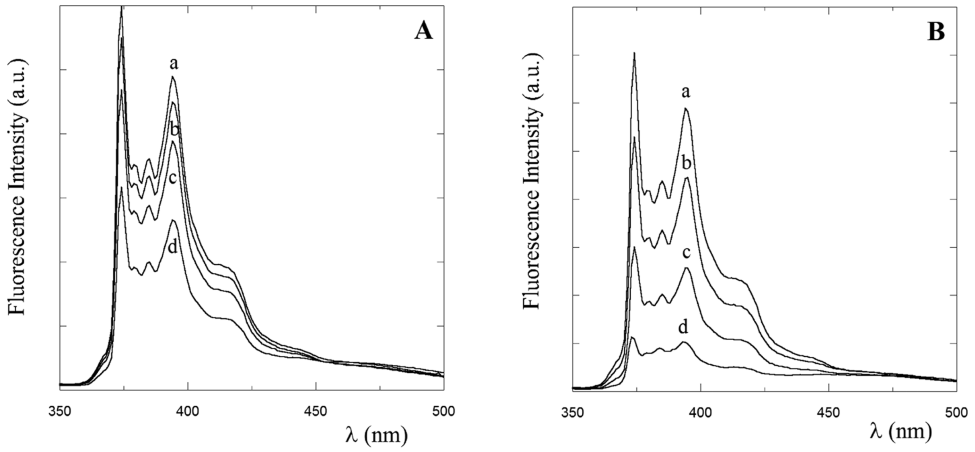

Figure 6. Fluorescence spectra of SSU6Py for different concentrations of TEOA (electron donor) (A) and MV^{2+} (electron acceptor) (B). Concentrations of TEOA or MV^{2+}: (a) 0 mM, (b) 0.5 mM, (c) 1.5 mM, and (d) 5 mM.

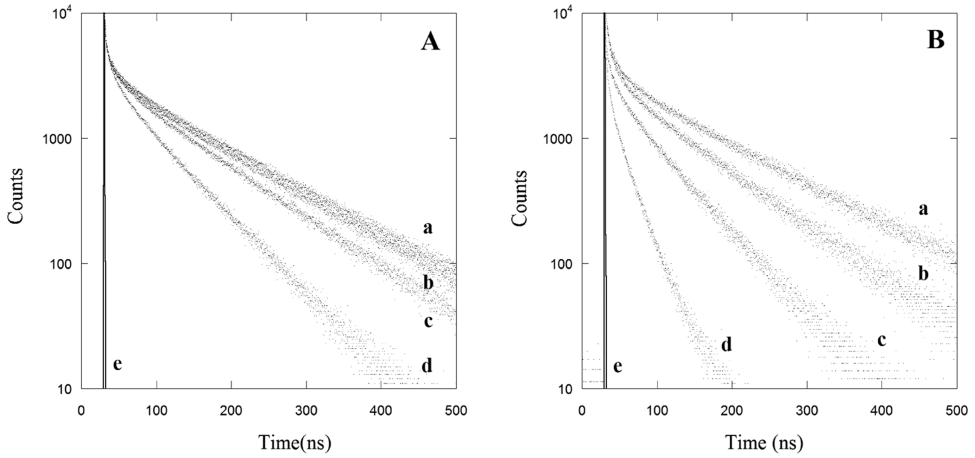

Figure 7. Fluorescence time decays of SSU6Py for different concentrations of TEOA (electron donor) (A) and MV^{2+} (electron acceptor) (B). Concentrations of TEOA or MV^{2+}: (a) 0 mM, (b) 0.5 mM, (c) 1.5 mM, and (d) 5 mM. (e) Excitation profile (λ_{exc} = 340 nm; λ_{em} = 397 nm).

where the Au−S and peptide polarities counterbalance their effects.[13]

The weak photocurrent signal observed in the case of the SSU6 SAM modified electrode is most probably related to a residual activity of MV^{2+} at the experimental wavelength (λ = 340 nm) or to the already mentioned photothermal effect, i.e., the current generated by the potential drop at the electrode surface caused by the temperature jump raised by the surface illumination.

Interestingly, when the photocurrent efficiencies reported in Figure 4A,B (see also Figure 2A,B) are compared, it clearly appears that the current intensities under anodic conditions are at least 1 order of magnitude larger than those detected under cathodic conditions. This finding confirms that ET through the peptide chain is the crucial step determining the overall PG efficiency and strengthens the aforementioned considerations on the influence of the helix macrodipole and the Au−S bond polarity regulating the directional character of this process.

It has been debated whether the superexchange coupling through the high-energy amide orbitals is more effective than hopping through the n and π ground-state orbitals. The efficiency of the latter mechanism shows a very weak decay with the D···A distance and is the only one still operative beyond 20 Å. However, at the short distances sampled by the hexapeptide SAM studied here, its efficiency is generally much lower than that attained by superexchange coupling.[5,12,55] The latter should be therefore considered as the predominant ET mechanism for the systems investigated in this work.

Fluorescence Experiments. Fluorescence experiments provided important information on the interaction taking place among the peptide building blocks forming the SSU6Py SAM, and in particular among the pyrene units functionalizing the oligopeptides at the C-terminus. In Figure 5A the fluorescence spectrum of the SSU6Py SAM immobilized on a quartz support coated by a 10 nm thick gold film is reported. In the spectrum a broad emission peaked at 480 nm can be observed, together with the sharp peaks typical of the pyrene monomer emission at 373 and 393 nm. The long-wavelength emission is characteristic of excimer species, i.e., fluorescent excited-state complexes formed by pyrene···pyrene interactions.[56] This finding is a clear indication of the densely packed nature of the SAM formed by SSU6Py on the gold surface. To confirm the intermolecular origin of the interaction leading to excimer emission, we carried out fluorescence experiments on the bicomponent SAM formed by overnight deposition of a 1:10 SSU6Py/SSU6 ethanol solution (5×10^{-5} and 5×10^{-4} M, respectively). The relative emission spectrum, also reported in Figure 5A, clearly reveals the absence of fluorescent excimer species, indicating that SSU6Py is homogeneously diluted in

dx.doi.org/10.1021/jp503791w | J. Phys. Chem. A 2014, 118, 6674−6684

Table 1. Time Decay Parameters of SSU6Py for Different Concentrations of TEOA or MV^{2+} Electron-Transfer Quenchers (λ_{exc} = 340 nm, λ_{em} = 397 nm)

[TEOA] (mM)	α_1	τ_1 (ns)	α_2	τ_2 (ns)	α_3	τ_3 (ns)	$\langle\tau\rangle$ (ns)	χ^2
0	0.61	1.2	0.16	18.2	0.23	129.5	33.4	1.33
0.5	0.61	1.4	0.16	18.8	0.23	123.6	32.3	1.26
1.5	0.62	1.7	0.16	18.4	0.22	106.5	27.4	1.21
5.0	0.64	1.5	0.16	12.8	0.20	66.8	16.4	1.32
[MV^{2+}] (mM)	α_1	τ_1 (ns)	α_2	τ_2 (ns)	α_3	τ_3 (ns)	$\langle\tau\rangle$ (ns)	χ^2
0	0.60	1.4	0.15	20.0	0.25	136.3	37.9	1.33
0.5	0.60	1.6	0.16	18.3	0.24	102.8	28.5	1.22
1.5	0.61	1.6	0.16	14.5	0.23	68.3	19.0	1.25
5.0	0.62	1.2	0.20	6.7	0.18	28.0	7.1	1.08

the SSU6 SAM, without formation of SSU6Py segregated domains.

To investigate how excimer formation could affect or interfere with the photoinduced ET process, photocurrent generation experiments were also carried out for the 1/10 SSU6Py/SSU6 SAM under both anodic (TEOA solution) and cathodic (MV^{2+} solution) conditions. The photocurrent action spectrum of the bicomponent SAM in a TEOA solution (Figure 5B) closely compares with the action spectrum of SSU6Py measured under anodic conditions (Figure 3A), well reproducing the absorption spectrum of pyrene.

Interestingly, the measured photocurrent intensity ratio between the SSU6Py and the 1/10 SSU6Py/SSU6 films is 4.5:1, which indicates a marked difference in the photocurrent efficiencies of the two systems, especially in view of the fact that combined CV and fluorescence experiments show that the pyrene content in the former is 1.3×10^{-10} mol/cm^2, whereas in the bicomponent SAM is only 1×10^{-11} mol/cm^2 (total peptide density 6×10^{-11} mol/cm^2).[27] This finding strongly suggests that in the SSU6Py SAM the electromagnetic excitation energy is largely dissipated in the processes leading to excimer formation and decay, i.e., self-quenching by energy transfer among the pyrene groups.[57]

Fluorescence experiments in solution allowed us to determine the bimolecular rate constant associated with the ET interaction between the pyrene excited state and the TEOA or MV^{2+} quencher molecules. The emission spectra of SSU6Py for different concentrations of the TEOA (ET donor) and MV^{2+} (ET acceptor) compounds are reported in Figure 6A,B for comparison. It can be observed that, in both cases, the SSU6Py emission is strongly quenched by the two compounds. The low emission measured between 450 and 500 nm indicates that formation of excimer or exciplex species at micromolar concentrations is minor, but not negligible.

The strong emission quenching detected by steady-state measurements was confirmed by time-resolved fluorescence experiments, as shown in Figure 7A,B, where the SSU6Py time decays for different concentrations of the TEOA and MV^{2+} quenchers are reported.

The experimental time decays can be described by discrete multiexponential lifetimes τ_i, i.e.

$$I(t) = \sum_i \alpha_i \exp\left(-\frac{t}{\tau_i}\right)$$

where α_i is the weight associated with the ith lifetime, proportional to the excited-state population at $t = 0$. In all cases, at least three lifetime components were necessary to adequately fit the experimental time decays, as often found for pyrene-labeled biomolecules.[58] An average time decay can be also introduced as the weighted-sum of the lifetime components, i.e., $\langle\tau\rangle = \Sigma_i \alpha_i \tau_i$. The parameters obtained by the time-resolved fluorescence experiments in SSU6Py/TEOA and SSU6Py/MV^{2+} solutions are reported in Table 1.

The efficiency of the ET process can be readily obtained from both spectral and time-resolved fluorescence experiments: from the former experiments through the equation

$$E_{ss} = 1 - \frac{\phi}{\phi_0}$$

where Φ and Φ_0 represent the fluorescence quantum yield in the presence and absence of the quencher molecules, respectively, and from the latter experiments through the equivalent equation

$$E_{dyn} = 1 - \frac{\langle\tau\rangle}{\tau_0}$$

where τ_0 is the SSU6Py excited-state lifetime in the absence of the quencher molecule.

The bimolecular rate constants for the SSU6Py*/TEOA and SSU6Py*/MV^{2+} ET interactions can be obtained from the quenching efficiencies from the equation

$$k_{ET} = \frac{1}{\tau_0[Q]}\left(\frac{E_{ss/dyn}}{1 - E_{ss/dyn}}\right)$$

The ET efficiencies and ET rate constants obtained from steady-state (E_{ss}, k_{ss}) and time-resolved (E_{dyn}, k_{dyn}) fluorescence experiments are reported in Table 2.

The fair agreement between E_{ss} and E_{dyn} confirms the excited-state character of the interactions involving SSU6Py* and the TEOA and MV^{2+} compounds. It should be noted that

Table 2. Electron-Transfer Quenching Efficiencies and Rate Constants from Steady-State (E_{ss}, k_{ss}^{ET}) and Time-Resolved (E_{dyn}, k_{dyn}^{ET}) Fluorescence Experiments

[TEOA] (mM)	E_{ss}	E_{dyn}	k_{ss}^{ET} (M^{-1} s^{-1}) ($\times 10^9$)	k_{dyn}^{ET} (M^{-1} s^{-1}) ($\times 10^9$)
0.5	0.08	0.03	5.2	1.9
1.5	0.22	0.18	5.6	4.4
5.0	0.47	0.51	5.3	6.2
[MV^{2+}] (mM)	E_{ss}	E_{dyn}	k_{ss}^{ET} (M^{-1} s^{-1}) ($\times 10^{10}$)	k_{dyn}^{ET} (M^{-1} s^{-1}) ($\times 10^{10}$)
0.5	0.33	0.24	2.6	1.7
1.5	0.57	0.50	2.3	1.8
5.0	0.85	0.81	3.0	2.2

dx.doi.org/10.1021/jp503791w | J. Phys. Chem. A 2014, 118, 6674−6684

the obtained ET rate constants are in the order of 10^{10} M^{-1} s^{-1} [$2.6(\pm0.2) \times 10^{10}$ from E_{ss} and $1.9(\pm0.2) \times 10^{10}$ M^{-1} s^{-1} from E_{dyn}] in the case of the MV^{2+} acceptor and 10^9 M^{-1} s^{-1} [$5.4(\pm0.2) \times 10^9$ from E_{ss} and $4.1(\pm1.8) \times 10^9$ M^{-1} s^{-1} from E_{dyn}] for the TEOA donor, respectively. The high value of the bimolecular ET rate constants strongly suggests that the rate-limiting step in the photocurrent generation experiment is ET through the peptide chain.

This finding is also confirmed by the already reported results of PG experiments in an equimolar TEOA/MV^{2+} solution, where a predominant anodic current was observed at all applied overpotentials, despite the 1 order of magnitude larger rate constant obtained in the case of the SSU6Py*/MV^{2+} ET as compared to that for SSU6Py*/TEOA ET. This finding further emphasizes the role of the electrostatic field of the helix macrodipole and the polarity of the Au−S linkage in determining the efficiency of the competitive ET processes through peptide SAMs supported on gold substrates. Therefore, the fine balance of anodic and cathodic currents shown by our PG experiments are the macroscopic consequence of the asymmetric ET through peptide helices at the molecular level.

CONCLUSIONS

In this contribution, PET processes through SAMs formed by helical oligopeptides suitably functionalized with a photosensitizing agent and chemisorbed on gold electrodes by a disulfide group are discussed. The aim of this study is to investigate the origin of the asymmetric ET efficiency through the peptide layer on going from the pyrene chromophore to gold or in the opposite direction. This study was accomplished by PG experiments carried out in a Grätzel-like electrochemical cell working under anodic (electron donor in solution) or cathodic (electron acceptor in solution) conditions.

Remarkably, the efficiency of PG for the SSU6Py SAM is 2 orders of magnitude larger than the photocurrent measured for a bare gold electrode or a gold electrode modified by the same peptide SAM, but lacking the pyrene chromophore (SSU6). The latter weak photocurrent was ascribed to a photothermal effect, i.e., the reorganization of the double-layer at the electrode surface in response to the temperature jump caused by the surface illumination.[52] Even more strikingly, and with more important consequences on both the theoretical and applicative points of view, is the strongly directional character of ET through the peptide chain. This effect can be ascribed to two fundamental properties of the systems investigated: (i) the electrostatic field generated by the peptide helices, arising from the ordered alignment of the single residue dipole moments in such structural arrangement, and (ii) the asymmetric charge injection barrier for ET at the interface between the metal electrode and the organic layer, due to the polar character of the Au−S ($Au^{\delta+}$−$S^{\delta-}$) interaction.

These properties could be usefully exploited for the development of organic/inorganic hybrid materials for molecular electronics or bioinspired optoelectronics. A DSSC prototype based on peptide materials has been recently produced in our laboratory.[43]

ASSOCIATED CONTENT

Supporting Information

Cyclic voltammetry of SSU6Py showing the formation of dihydroxypyrene (Figure SI1); photocurrent action spectra of (Au)SSU6Py in an equimolar TEOA and MV^{2+} solution at 0 V applied potential (inset: photocurrent intensity/applied voltage dependence of the same experiment) (Figure SI2). This material is available free of charge via the Internet at http://pubs.acs.org.

AUTHOR INFORMATION

Corresponding Author

*M. Venanzi: e-mail, venanzi@uniroma2.it.

Notes

The authors declare no competing financial interest.

ACKNOWLEDGMENTS

The financial support of the Italian Minister of University and Research (MIUR) for the project PRIN 2010-2011 no. 2010FM738P, "Photophysical and photochemical properties of organic and biological compounds in solution and in organized systems", is gratefully acknowledged.

REFERENCES

(1) Isied, S. S.; Ogawa, M. Y.; Wishart, J. F. Peptide-Mediated Intramolecular Electron Transfer: Long-Range Distance Dependence. *Chem. Rev.* **1992**, *92*, 381−394.
(2) Gray, H. B.; Winkler, J. R. Electron Transfer through Proteins. *Q. Rev. Biophys.* **2003**, *36*, 341−372.
(3) Gray, H. B.; Winkler, J. R. Long-Range Electron Transfer. *Proc. Natl. Acad. Sci. U. S. A.* **2005**, *102*, 3534−3539.
(4) Cordes, M.; Giese, B. Electron Transfer in Peptides and Proteins. *Chem. Soc. Rev.* **2009**, *38*, 892−901.
(5) Sisido, M.; Hoshino, S.; Kusano, H.; Kuragaki, M.; Makino, M.; Sasaki, H.; Smith, T. A.; Ghiggino, K. P. Distance Dependence of Photoinduced Electron Transfer along α-Helical Polypeptides. *J. Phys. Chem. B* **2001**, *105*, 10407−10415.
(6) Morita, T.; Kimura, S. Long-Range Electron Transfer over 4 nm Governed by an Inelastic Hopping Mechanism in Self-Assembled Monolayers of Helical Peptides. *J. Am. Chem. Soc.* **2003**, *125*, 8732−8733.
(7) Malak, R. A.; Gao, Z.; Wishart, J. F.; Isied, S. S. Long-Range Electron Transfer across Peptide Bridges: the Transition from Electron Superexchange to Hopping. *J. Am. Chem. Soc.* **2004**, *126*, 13888−13889.
(8) Cordes, M.; Köttgen, A.; Jasper, C.; Jacques, O.; Boudebous, H.; Giese, B. Influence of Amino Acid Side-chains on Long-Distance Electron Transfer in Peptides: Electron Hopping via "Stepping Stones". *Angew. Chem.* **2008**, *47*, 3461−3463.
(9) Antonello, S.; Formaggio, F.; Moretto, A.; Toniolo, C.; Maran, F. Anomalous Distance Dependence of Electron Transfer across Peptide Spacers. *J. Am. Chem. Soc.* **2003**, *125*, 2874−2875.
(10) Polo, F.; Antonello, S.; Formaggio, F.; Toniolo, C.; Maran, F. Evidence against the Hopping Mechanism as an Important Electron Transfer Pathway for Conformationally Constrained Oligopeptides. *J. Am. Chem. Soc.* **2005**, *127*, 492−493.
(11) Gatto, E.; Venanzi, M. Peptronics: Peptide Materials for Electron Transfer. In *Peptide Materials: from Nanostructures to Applications*; Aleman, C., Bianco, A., Venanzi, M., Eds.; Wiley: Chichester, U.K., 2013; pp 105−147.
(12) Long, Y.-T.; Abu-Irhayem, E.; Kraatz, H. B. Peptide Electron Transfer: More Questions than Answers. *Chem.—Eur. J.* **2005**, *11*, 5186−5194.
(13) Morita, T.; Kimura, S.; Kobayashi, S. Photocurrent Generation under a Large Dipole Moment Formed by Self-Assembled Monolayers of Helical Peptides Having an N-Ethylcarbazolyl Group. *J. Am. Chem. Soc.* **2000**, *122*, 2850−2859.
(14) Yanagisawa, K.; Morita, T.; Kimura, S. Efficient Photocurrent Generation by Self-Assembled Monolayers Composed of 3_{10}-Helical Peptides Carrying Linearly Spaced Naphthyl Groups at the Side Chains. *J. Am. Chem. Soc.* **2004**, *126*, 12780−12781.

(15) Yasutomi, S.; Morita, T.; Imanishi, Y.; Kimura, S. A Molecular Photodiode System that Can Switch Photocurrent Direction. *Science* **2004**, *304*, 1944−1947.
(16) Yasutomi, S.; Morita, T.; Kimura, S. pH-Controlled Switching of Photocurrent Detection by Self-Assembled Monolayer of Helical Peptides. *J. Am. Chem. Soc.* **2005**, *127*, 14564−14565.
(17) Kitagawa, K.; Morita, T.; Kimura, S. Electron Transfer in Metal-Molecule-Metal Junction Composed of Self-Assembled Monolayers of Helical Peptides Carrying Redox-Active Ferrocene Units. *Langmuir* **2005**, *21*, 10624−10631.
(18) Kitagawa, K.; Morita, T.; Kimura, S. Molecular Rectification of a Helical Peptide with a Redox Group in the Metal-Molecule-Metal Junction. *J. Phys. Chem. B* **2005**, *109*, 13906−13911.
(19) Takeda, K.; Morita, T.; Kimura, S. Effects of Monolayer Structures on Long-Range Electron Transfer in Helical Peptide Monolayer. *J. Phys. Chem. B* **2008**, *112*, 12840−12850.
(20) Arikuma, Y.; Takeda, K.; Morita, T.; Ohmae, M.; Kimura, S. Linker Effects on Monolayer Formation and Long-Range Electron Transfer in Helical Peptide Monolayers. *J. Phys. Chem. B* **2009**, *113*, 6256−6266.
(21) Arikuma, Y.; Nakayama, H.; Morita, T.; Kimura, S. Ultra-Long-Range Electron Transfer through a Self-Assembled Monolayer on Gold Composed of 120 Å-Long α-Helices. *Langmuir* **2011**, *27*, 1530−1535.
(22) Galka, M. M.; Kraatz, H. B. Electron Transfer Studies in Self-Assembled Monolayers of Helical Ferrocene-Oligoproline-Cystamine Bound to Gold. *ChemPhysChem* **2002**, *3*, 356−359.
(23) Orlowski, G. A.; Chowdhuri, S.; Kraatz, H. B. Reorganization Energies of Ferrocene-Peptide Monolayers. *Langmuir* **2007**, *23*, 12765−12770.
(24) Gatto, E.; Stella, L.; Formaggio, F.; Toniolo, C.; Lorenzelli, L.; Venanzi, M. Electroconductive and Photocurrent Generation Properties of Self-Assembled Monolayers Formed by Functionalized, Conformationally Constrained Peptides on Gold Electrodes. *J. Pept. Sci.* **2008**, *14*, 184−191.
(25) Gatto, E.; Stella, L.; Baldini, C.; Toniolo, C.; Formaggio, F.; Venanzi, M. Photocurrent Generation in Peptide-Based Self-Assembled Monolayers on Gold Electrodes. *Superlattices Microstruct.* **2009**, *46*, 34−39.
(26) Gatto, E.; Caruso, M.; Porchetta, A.; Toniolo, C.; Formaggio, F.; Crisma, M.; Venanzi, M. Photocurrent Generation through Peptide-Based Self-Assembled Monolayers on a Gold Surface: Antenna and Junction Effects. *J. Pept. Sci.* **2011**, *17*, 124−131.
(27) Gatto, E.; Porchetta, A.; Scarselli, M.; De Crescenzi, M.; Formaggio, F.; Toniolo, C.; Venanzi, M. Playing with Peptides: How to Build a Supramolecular Peptide Nanostructure by Exploiting Helix···Helix Macrodipole Interactions. *Langmuir* **2012**, *28*, 2817−2826.
(28) Sek, S.; Tolak, A.; Misicka, A.; Palys, B.; Bilewics, R. Asymmetry of Electron Transmission through Monolayers of Helical Polyalanine Adsorbed on Gold Surfaces. *J. Phys. Chem. B* **2005**, *109*, 18433−18438.
(29) Sek, S.; Swiatek, K.; Misicka, A. Electrical Behavior of Molecular Junctions Incorporating α-Helical Peptides. *J. Phys. Chem. B* **2005**, *109*, 23121−23124.
(30) Sek, S. Two Metal-Molecule Binding Modes for Peptide Molecules Junctions. *J. Phys. Chem. C* **2007**, *111*, 12860−12865.
(31) Xiao, X.; Xu, B.; Tao, N. Conductance Titration of Single Peptide Molecules. *J. Am. Chem. Soc.* **2005**, *126*, 5370−5371.
(32) Galoppini, E.; Fox, M. A. Effect of the Electric Field Generated by the Helix Dipole on Photoinduced Intramolecular Electron Transfer in Dichromophoric α-Helical Peptides. *J. Am. Chem. Soc.* **1996**, *118*, 2299−2300.
(33) Fox, M. A.; Galoppini, E. Electric Field Effect on Electron Transfer Rates in Dichromophoric Peptides: the Effect of Helix Unfolding. *J. Am. Chem. Soc.* **1997**, *119*, 5277−5285.
(34) Gatto, E.; Porchetta, A.; Stella, L.; Guryanov, I.; Formaggio, F.; Toniolo, C.; Kaptein, B.; Broxterman, Q. B.; Venanzi, M. Conformational Effects on the Electron Transfer Efficiency in Peptide Foldamers Based on α,α-Disubstituted Glycyl Residues. *Chem. Biodiv.* **2008**, *5*, 1263−1278.
(35) Gellman, S. H. Foldamers: A Manifesto. *Acc. Chem. Res.* **1998**, *31*, 173−180.
(36) Toniolo, C.; Crisma, M.; Formaggio, F.; Peggion, C. Control of Peptide Conformation by the Thorpe-Ingold Effect (C^{α}-Tetrasubstitution). *Biopolymers (Pept. Sci.)* **2001**, *60*, 396−419.
(37) Toniolo, C.; Crisma, M.; Bonora, G.; Benedetti, E.; Di Blasio, B.; Pavone, V.; Pedone, C.; Santini, A. Preferred Conformation of the Terminally Blocked $(Aib)_{10}$ Homo-Oligopeptide: A Long, Regular 3_{10}-Helix. *Biopolymers* **1991**, *31*, 129−138.
(38) Karle, I. L.; Balaram, P. Structural Characteristics of α-Helical Peptide Molecules Containing Aib Residues. *Biochemistry* **1990**, *29*, 6747−6756.
(39) Bolin, K. A.; Millhauser, G. L. α and 3_{10}: The Split Personality of Polypeptide Helices. *Acc. Chem. Res.* **1999**, *32*, 1027−1033.
(40) Pispisa, B.; Stella, L.; Venanzi, M.; Palleschi, A.; Viappiani, C.; Polese, A.; Formaggio, F.; Toniolo, C. Quenching Mechanisms in Bichromophoric, 3_{10}-Helical Aib-Based Peptides, Modulated by Chain-Length Dependent Topologies. *Macromolecules* **2000**, *33*, 906−915.
(41) Venanzi, M.; Pace, G.; Palleschi, A.; Stella, L.; Castrucci, P.; Scarselli, M.; De Crescenzi, M.; Formaggio, F.; Toniolo, C.; Marletta, G. Densely-Packed Self-Assembled Monolayers on Gold Surfaces from a Conformationally Constrained Helical Hexapeptide. *Surf. Sci.* **2006**, *600*, 409−416.
(42) Pace, G.; Venanzi, M.; Castrucci, P.; Scarselli, M.; De Crescenzi, M.; Palleschi, A.; Stella, L.; Formaggio, F.; Toniolo, C.; Marletta, G. Static and Dynamic Features of a Helical Hexapeptide Chemisorbed on a Gold Surface. *Mater. Sci. Eng., C* **2006**, *26*, 918−923.
(43) Gatto, E.; Quatela, A.; Caruso, M.; Tagliaferro, R.; De Zotti, M.; Formaggio, F.; Toniolo, C.; Di Carlo, A.; Venanzi, M. Mimicking the Nature: A Novel Peptide-Based Bio-Inspired Approach for Solar Energy Conversion. *ChemPhysChem* **2014**, *15*, 64−68.
(44) Kakiuchi, T.; Usui, H.; Hobara, D.; Yamamoto, M. Voltammetric Properties of the Reductive Desorption of Alkanethiol Self-Assembled Monolayers from a Metal Surface. *Langmuir* **2002**, *18*, 5231−5238.
(45) Bard, A. J.; Faulkner, L. R. *Electrochemical Methods*; John Wiley & Sons: Danvers, MA, 2001.
(46) Khazraji, A. C.; Hotchandani, S.; Das, S.; Kamat, P. V. Controlling Dye (Merocyanine-540) Aggregation on Nanostructured TiO_2 films. An Organized Assembly Approach for Enhancing the Efficiency of Photosensitization. *J. Phys. Chem. B* **1999**, *103*, 4693−4700.
(47) Kuhn, J. H.; Braslavsky, S. E.; Schmidt, R. Chemical Actinometry. *Pure Appl. Chem.* **1989**, *61*, 187−210.
(48) Pensa, E.; Cortés, E.; Corthey, G.; Carro, P.; Vericat, C.; Fonticelli, M. H.; Benitez, G.; Rubert, A. A.; Salvarezza, R. C. The Chemistry of the Sulfur-Gold Interface: In Search of a Unified Model. *Acc. Chem. Res.* **2012**, *45*, 1183−1192.
(49) Watanabe, J.; Morita, T.; Kimura, S. Effects of Dipole Moment, Linkers, and Chromophores at Side Chains on Long-Range Electron Transfer through Helical Peptides. *J. Phys. Chem. B* **2005**, *109*, 14416−14425.
(50) Wain, A. J.; Do, H. N. L.; Mandal, H. S.; Kraatz, H.-B.; Zhou, F. Influence of Molecular Dipole Moment on the Redox-Induced Reorganization of α-Helical Peptide Self-Assembled Monolayers: An Electrochemical SPR Investigation. *J. Phys. Chem. C* **2008**, *112*, 14513−14519.
(51) Miura, Y.; Kimura, S.; Kobayashi, S.; Iwamoto, M.; Imanishi, Y.; Umemura, J. Negative Surface Potential Produced by Self-Assembled Monolayers of Helix Peptides Oriented Vertically to a Surface. *Chem. Phys. Lett.* **1999**, *315*, 1−6.
(52) Mandal, H. S.; Burgess, I. J.; Kraatz, H. B. Investigation of Laser Induced Photocurrent Generation Experiments. *J. Chem. Soc., Chem. Commun.* **2006**, 4802−4804.
(53) Adams, D. M.; Brus, L.; Chidsey, C. E. D.; Creager, S.; Creutz, C.; Kagan, C. R.; Kamat, P. V.; Lieberman, M.; Lindsay, S.; Marcus, R. A.; Metzger, R. M.; Michel-Beyerle, M. E.; Miller, J. R.; Newton, M.

D.; Rolison, D. R.; Sankey, O.; Schanze, K. S.; Yardley, J.; Zhu, X. Charge Transfer on the Nanoscale: Current Status. *J. Phys. Chem. B* **2003**, *107*, 6668−6697.
(54) Mc Creery, R. L. Molecular Electronic Junctions. *Chem. Mater.* **2004**, *16*, 4477−4496.
(55) Kai, M.; Takeda, K.; Morita, T.; Kimura, S. Distance Dependence of Long-Range Electron Transfer through Helical Peptides. *J. Pept. Sci.* **2008**, *14*, 192−202.
(56) Winnik, F. M. Photophysics of Preassociated Pyrenes in Aqueous Polymer Solutions and Other Organized Media. *Chem. Rev.* **1993**, *93*, 587−614.
(57) Spitler, M. T. Quenching of Dye-Sensitized Photocurrent at Zinc Oxide Conductor Electrodes. *J. Phys. Chem.* **1986**, *90*, 2156−2159.
(58) Yao, C.; Kraatz, H.-B.; Steer, R. P. Photophysics of Pyrene-Labelled Compounds of Biological Interest. *Photochem. Photobiol. Sci.* **2005**, *4*, 191−199.